BIOCELL

Tech Science Press

http://doi.org/10.32604/biocell.2026.081668

ARTICLE

Fibroblast-Secreted GDF11 Regulates Osteoclast Differentiation in Middle Ear Cholesteatoma through the SMAD2/3 Pathway by Targeting TGFBR1

Zhikai Wang[1], Xing Wang[2], Lun Dong[1], Wei Wang[1] and Xiaoping Gao[1,*]

[1]Department of Otorhinolaryngology Head and Neck Surgery, General Hospital of Ningxia Medical University, Yinchuan, China
[2]Outpatient Department, Ningxia Minkang Hospital, Yinchuan, China
*Corresponding Author: Xiaoping Gao. Email: monsieurgao@163.com

Received: 06 March 2026; Accepted: 16 June 2026; Published: 22 September 2026

ABSTRACT: Objectives: Middle ear cholesteatoma (MEC) is a destructive and locally invasive disease that leads to erosion of bone structure and serious complications. This study aimed to investigate the role of GDF11 in promoting the differentiation of macrophages into osteoclasts *in vitro* and elucidate the bone erosion mechanism in MEC. **Methods:** The MEC dataset GSE116142 was subjected to bioinformatics analysis. The Growth Differentiation Factor 11 (GDF11) and Transforming Growth Factor Beta Receptor 1 (TGFBR1) expression levels in MEC were evaluated using immunohistochemical analysis. RAW264.7 cells were induced with different concentrations of recombinant GDF11 (rGDF11) with or without the TGFBR1 inhibitor AZ12601011. *Gdf11*-overexpressing and *Gdf11* knockdown NIH-3T3 cell lines were constructed and co-cultured with RAW264.7 cells. Tartrate-resistant acid phosphatase (TRAP) staining was performed to identify TRAP-positive cells. The expression levels of GDF11, TGFBR1, and osteoclast-related markers were determined using reverse transcription-quantitative polymerase chain reaction and western blotting analyses. **Results:** GDF11 and TGFBR1, which were significantly upregulated in MEC ($p < 0.05$), were enriched in cytokine-cytokine receptor interaction and osteoclast differentiation. Treatment with AZ12601011 mitigated the rGDF11-induced upregulation of TRAP-positive cell number ($p < 0.01$) and TGFBR1 ($p < 0.01$), *Trap* ($p < 0.01$), and phosphorylated Mothers Against Decapentaplegic Homolog (Smad) 2/3 levels ($p < 0.01$) and upregulated osteoclast-related factors ($p < 0.05$). The number of $TRAP^+$ cells ($p < 0.01$), the secretion of GDF11 ($p < 0.01$), and the expression levels of Gdf11 ($p < 0.01$), Tgfbr1 ($p < 0.01$), and Nfatc1 ($p < 0.01$) were significantly upregulated in the *Gdf11*-overexpressing fibroblast/macrophage co-culture. In the co-culture system with *Gdf11* knockdown or AZ12601011 treatment, Gdf11-induced changes were mitigated ($p < 0.05$). **Conclusion:** GDF11 upregulation in fibroblasts enhances GDF11 secretion, promoting the differentiation of macrophages into osteoclasts. The elucidation of this intercellular communication can aid in developing therapeutic interventions for MEC-related bone erosion.

KEYWORDS: Middle ear cholesteatoma; bone erosion; osteoclast differentiation; growth differentiation factor 11; transforming growth factor beta receptor 1; mothers against decapentaplegic homolog 2/3

1 Introduction

Middle ear cholesteatoma (MEC) is a cystic lesion lined by keratinizing stratified squamous epithelium (primarily involving the epitympanum or mastoid air cells) and surrounded by a fibrous tissue layer (perimatrix) of variable thickness [1,2]. Although MEC is considered benign, it can destroy the ossicular chain, otic capsule, and other surrounding bone structures, resulting in serious complications, such as conductive hearing loss, vestibular dysfunction, facial paralysis, and meningitis [3]. The only definitive

treatment for MEC is surgery [3]. The elucidation of cellular drivers of bone resorption in MEC will enable the development of non-invasive interventions for osteolysis.

Progressive osteolytic bone destruction, a hallmark clinical feature of MEC, involves an imbalance between bone resorption and bone formation. Osteoclasts serve as the primary effector cells driving pathological bone resorption [4]. Previous studies have demonstrated that mature osteoclasts infiltrate MEC lesions and actively drive bone destruction. Mature osteoclasts adhere to resorption lacunae beneath the cholesteatoma matrix, promoting bone degradation by secreting acids and proteases (such as CTSK) through their ruffled borders [5]. The osteoclastic activity induces measurable microstructural changes (increased porosity in incus specimens) [6]. Previous studies have attempted to elucidate the mechanisms of osteoclast-mediated bone resorption, although the exact pathways in MEC are unclear.

The RANK/RANKL/OPG axis serves as the master regulatory mechanism of osteoclastogenesis. The binding of receptor activator of nuclear factor κB ligand (RANKL) to RANK on the osteoclast precursor surface induces the activation of NF-κB and NFATC1, promoting differentiation into mature osteoclasts. Meanwhile, osteoprotegerin (OPG) functions as a decoy receptor to inhibit osteoclast differentiation [7,8]. Transforming growth factor (TGF)-β signaling plays dual roles in bone homeostasis, promoting osteoclastogenesis through Mothers Against Decapentaplegic Homolog (SMAD) 2/3-dependent pathways and inhibiting this process through SMAD1/5/8 activation [9,10]. Growth differentiation factor 11 (GDF11), also called bone morphogenetic protein 11 (BMP11), is a member of the TGF-β superfamily [11]. Previous studies have indicated that GDF11 mediates diverse biological processes, including lipid metabolism [12], neurogenesis [13], maintenance of stem cell characteristics [14], and cell cycle regulation [15]. GDF11 is involved in regulating the growth and differentiation of bone cell lineages and consequently mediating skeletal development and bone metabolism. Additionally, GDF11 is reported to serve as a protective factor for osteoblast generation by targeting PPAR-γ [16]. However, GDF11 can also inhibit the differentiation of bone marrow mesenchymal stem cells into osteoblasts [17–19]. Additionally, GDF11 can exacerbate hip joint dysplasia by inhibiting chondrocyte proliferation and hypertrophy [20]. However, the role of GDF11 in MEC is unclear.

Osteoclast differentiation is modulated within the stroma surrounding cholesteatoma [1]. A previous study utilized the cholesteatoma model and an *in vitro* co-culture system to confirm that keratinocytes can promote osteoclast differentiation by upregulating RANKL in fibroblasts [21]. Gong et al. further demonstrated that miRNA-17 can target *TNFSF11* to regulate RANKL expression in fibroblasts through keratinocyte exosomes isolated from patients with MEC [22]. The interactions between these cells are crucial for the local regulation of osteoclast activation and recruitment in MEC [23]. However, the mechanisms underlying this process have not been elucidated.

Bioinformatics analysis of Gene Expression Omnibus (GEO) datasets revealed that the expression levels of GDF11 and its type I receptor Alk5 (TGFBR1) are upregulated in the perimatrix of MEC. By contrast, other type I receptors that mediate GDF11 signaling, such as ACVR2B and ALK4, were not identified as differentially expressed genes in the same dataset, prompting us to focus on TGFBR1. This study hypothesized that GDF11 promotes the differentiation of macrophages into osteoclasts by specifically activating TGFBR1 on the fibroblast surface, initiating a cascade reaction in the SMAD2/3 signaling pathway. In this study, the expression levels of GDF11 and TGFBR1 in clinical MEC samples were evaluated using immunohistochemical analysis. Next, RAW264.7 cells were exogenously treated with recombinant GDF11 (rGDF11) in combination with the key cytokines macrophage colony-stimulating factor (M-CSF) and RANKL to investigate the impact of GDF11 on the differentiation of macrophages into osteoclasts. Furthermore, a co-culture system of fibroblasts and macrophages was established to elucidate the signaling mechanism

through which GDF11 activates the TGFBR1-SMAD2/3 axis in fibroblasts, as well as to investigate its paracrine effects on the differentiation of macrophages into osteoclasts.

2 Methods

2.1 MEC Dataset

The study flowchart is shown in Fig. A1. The GSE116142 dataset, which was downloaded from the GEO database at the National Center for Biotechnology Information website (https://www.ncbi.nlm.nih.gov/geo/), comprises the data of samples collected from patients undergoing tympanomastoidectomy. In particular, the dataset comprised the high-throughput sequencing data of cholesteatoma perimatrix and retroauricular dermis [1].

2.2 Bioinformatic Analysis of the Transcriptome

Differentially expressed genes (DEGs) were analyzed using the R software (version 4.2.2) with 'limma' package (version 3.54.0) based on the following criteria: $p < 0.05$ and $|\log_2$ fold-change (FC)$| > 1$. The heatmaps and volcano plots were generated using the 'pheatmap' (version 1.0.13) and 'ggplot2' (version 4.0.1) R packages, respectively. These visual representations highlighted the DEGs, their significance levels, and FCs. DEGs were subjected to Gene Ontology (GO) and Kyoto Encyclopedia of Genes and Genomes (KEGG) functional enrichment analyses using the 'clusterProfiler' package (version 4.18.0). Furthermore, gene set enrichment analysis (GSEA) was performed with a significance threshold set at $p < 0.05$.

The expression levels of target genes, including *GDF11* and *TGFBR1*, between the control and MEC samples were compared using the *t*-test. Additionally, the STRING database (https://cn.string-db.org/) was used to verify the interaction between GDF11 and TGFBR1 (Score: 0.999).

2.3 Patients and Samples

This study was approved by the Medical Research Ethics Review Committee of the General Hospital of Ningxia Medical University (Approval No.: KYLL-2021-612) in accordance with the Declaration of Helsinki. This study analyzed samples from eight patients with MEC, comprising four males and four females, who underwent surgical resection at the General Hospital of Ningxia Medical University between January 2022 and December 2023 (Table A1). The patients ranged in age from 21 to 69 years, with a mean age of 46.6 years. Retroauricular skin tissue from the same patients served as controls. All patients were diagnosed with acquired secondary cholesteatoma. Written informed consent was obtained from the patients to use their samples. Some collected samples were embedded in paraffin samples for immunohistochemical analysis, while some samples were immediately stored in liquid nitrogen for molecular analysis.

2.4 Immunohistochemical Analysis

The expression patterns of GDF11 and TGFBR1 in MEC and retroauricular skin tissues were determined using immunohistochemical analyses. The paraffin-embedded samples (thickness: 4 μm) were incubated with ethylenediaminetetraacetic acid-citrate buffer (pH 8.0) in a 90°C water bath for 30 min for antigen retrieval. Next, the sections were blocked with 3% bovine serum albumin for 30 min at room temperature and incubated with anti-GDF11 antibodies (1:100, BM4892, BOSTER, Pleasanton, CA, USA; TGFBR1: 1:600, GB114126 Servicebio, Wuhan, China) at 4°C overnight. The sections were then incubated with horseradish peroxidase (HRP)-conjugated secondary antibodies (GB23303, 1:200, Servicebio, Wuhan, China) at room temperature for 50 min. Immunoreactive signals were developed using the substrate 3,3′-diaminobenzidine (concentration: 0.05% DAB, 0.03% H_2O_2 in PBS, applied for 2–5 min at room temperature in the dark). The

reaction progress was monitored under a light microscope (BX53, Olympus, Tokyo, Japan). The formation of a brownish-yellow color indicated positive results.

2.5 Cell Culture and Treatment

The mouse macrophages (RAW264.7 cells) and the mouse fibroblasts (NIH-3T3 cells), which were obtained from Procell in Wuhan, China, were cultured in high-sugar Dulbecco's modified Eagle's medium (DMEM) (C3113-0500, VivaCell, Shanghai, China) supplemented with 10% fetal bovine serum (FBS; 04-001-1ACS, Biological Industries, kibbutz beit-haemek, Israel) and 1% penicillin/streptomycin (P/S, C3421-0100, VivaCell) at 37°C. NIH-3T3 cells were cultured in DMEM supplemented with 10% newborn calf serum (16010159, Gibco, Carlsbad, CA, USA) and 1% P/S. Both cell lines were authenticated by short tandem repeat (STR) profiling and tested negative for mycoplasma contamination.

2.5.1 Osteoclast Differentiation

The RAW264.7 cells were enzymatically dissociated using trypsin (0.25% trypsin with 0.02% EDTA, C3530-0100, VivaCell, Shanghai, China) and resuspended to a concentration of 3×10^5 cells/mL. After incubating overnight, cells were cultured in a medium containing 100 ng/mL RANKL and 25 ng/mL M-CSF to induce osteoclast differentiation. To examine the effect of GDF11, cells in the osteoclast differentiation medium were incubated with 10 or 50 ng/mL of rGDF11 [17]. Further, the cells were incubated with the TGFBR1 inhibitor AZ12601011 at a concentration of 20 nM [24]. RANKL (HY-P7425), M-CSF (HY-P7085), rGDF11 (HY-P70222), and AZ12601011 (HY-122856) were purchased from MCE, Shanghai, China. The RAW264.7 cells were incubated at 37°C in a 5% CO_2 incubator (Forma 371, Thermo, Asheville, NC, USA) for 4 days to induce osteoclast differentiation. The culture medium was replaced once every two days.

2.5.2 Lentiviral Infection

The overexpression sequence was cloned into the lentiviral vector JS036 (Justscience Biotech, Shanghai, China). Meanwhile, the short hairpin construct against GDF11 (shGDF11; 5′-GATCCCGTATCCGTTCACT AAAGATTCTCGAGAATCTTTAGTGAACGGATACGTTTTTG-3′) was cloned into the lentiviral vector JS040 (Justscience Biotech, Shanghai, China). The empty vectors (negative control (NC) and shNC) were used as controls. NIH-3T3 cells at the logarithmic growth phase were dissociated using trypsin (0.25% trypsin with 0.02% EDTA, C3530-0500, VivaCell, Shanghai, China), plated in a six-well plate (2.5×10^4 cells/mL), and cultured overnight. Lentiviral constructs were transduced into cells at a multiplicity of infection of 50 in a complete culture medium supplemented with HitransG P infection enhancer (REVG005, GENECHEM, Shanghai, China). At 72 h post-transfection, the culture medium was replaced with complete DMEM containing 3 μg/mL puromycin dihydrochloride (HY-B1743A, MCE) to select for stably transduced cells over 48 h. The transduction efficiency was evaluated using reverse transcription-quantitative polymerase chain reaction (RT-qPCR) and western blotting analyses. The cells were digested with trypsin, passaged, and cultured in complete DMEM.

2.5.3 Co-Culture Assay

RAW264.7 cells were subjected to trypsinization (0.25% trypsin-EDTA), counted, and plated (3×10^5 cells/mL) in the lower chamber of a 0.4 μm polycarbonate plug-in cell culture (140640, Corning Inc., Corning, NY, USA). NIH-3T3 cells (1×10^5 cells/mL) were seeded into the upper chamber of the Transwell system. The medium in the upper chamber was replaced with fresh medium once every three days for 6–7 days. Meanwhile, the culture medium in the lower chamber was replaced with fresh medium supplemented with 100 ng/mL RANKL

and 25 ng/mL M-CSF once every 2 days. Cell morphology was monitored once every 2 days. Additionally, the NIH-3T3 cells were selectively treated with 20 nM AZ12601011 for 48 h. The culture supernatant from the lower chamber was collected to measure the concentration of Gdf11 using the enzyme-linked immunosorbent assay (ELISA). RAW264.7 cells were harvested for RT-qPCR, western blotting, and tartrate-resistant acid phosphatase (TRAP) staining analyses.

2.6 TRAP Staining

The RAW264.7 cells after co-culture were stained using a TRAP staining kit (G1050-50T, Servicebio) to identify osteoclasts. Briefly, after aspirating the culture medium, the cells were fixed using 4% paraformaldehyde solution (G1101-500 mL, Servicebio) and permeabilized with 0.2% Triton X-100 (0694, Amresco, Solon, OH, USA) for 15 min. Next, the cells were incubated with TRAP solution at 37°C in the dark for 1 h. The cells were then dehydrated using anhydrous ethanol, mounted in reverse on clean glass slides using neutral resin for sealing, and observed under a microscope (RVL-100-G, ECHO Laboratories, San Diego, CA, USA). The images were captured in five random fields to count $TRAP^+$ cells.

2.7 RT-qPCR Analysis

Total RNA was extracted from cultured cells (i.e., RAW264.7 cells and NIH-3T3 cells) or clinical samples using Trizol reagent (R0016, Beyotime, Shanghai, China). The RNA in the lysate was purified using the phenol-chloroform method. The purified RNA was reverse-transcribed into complementary DNA (cDNA) using the high-capacity cDNA Archive kit (4368814, Applied Biosystems, Waltham, MA, USA). RT-qPCR analysis was performed using an A7900HT Sequence Detector System (Applied Biosystems, Foster City, CA, USA) with the ChamQ Universal SYBR qPCR Master Mix (Q711-02, Vazyme, Nanjing, China). Melting curve analysis was performed to confirm the specificity of each amplicon. The mRNA expression levels of *TRAP*, *NFATC1*, *GDF11*, and *TGFBR1* were normalized to those of *GAPDH*. The relative gene expression levels were calculated using the $2^{-\Delta\Delta Ct}$ method. The specific primer pairs are listed in Table 1.

Table 1: The sequences of the specific primers for the target gene.

Primer	Sequence (5′→3′)
H-GDF11-F	ACAAGGCCAACTACTGCTCC
H-GDF11-R	CTGCACCAAATGGGTATGCG
H-TGFBR1-F	TCCAACTACTGGCCCTTTTTCA
H-TGFBR1-R	ATGGTGAATGACAGTGCGGT
H-TRAP-F	CGTATTCTCTGACCGCTCCC
H-TRAP-R	TGCCAAGGTGGTCATGGTTT
H-NFATC1-F	CTCTGGTGGTTGAGATCCCG
H-NFATC1-R	CGTATTATTTCATTTACGTTGGCGG
H-GAPDH-F	GTTCGTCATGGGTGTGAACC
H-GAPDH-R	CATCCACAGTCTTCTGGGTG
M-Gdf11-F	CAGCCTGAGGACTTCTTG
M-Gdf11-R	TGAACGGATACGGATGTG
M-Tgfbr1-F	CGACGCTGTTCTATTGGT
M-Tgfbr1-R	CTGTTGGCTGAGTTGTGA
M-Trap-F	AGAACTTGCGACCATTGT
M-Trap-R	TCCAGAGGCTTCCACATA
M-Gapdh-F	TCTCCTGCGACTTCAACA
M-Gapdh-R	TGTAGCCGTATTCATTGTCA

2.8 Western Blotting Analysis

Total proteins were extracted from cultured cells (RAW264.7 cells or NIH-3T3 cells) or clinical samples using radioimmunoprecipitation assay buffer (P0013, Beyotime) on ice. The protein concentration was quantified using a BCA protein assay kit (P0012, Beyotime, Shanghai, China) according to the manufacturer's instructions. The protein samples were denatured at 95°C for 5 min and subjected to sodium dodecyl sulfate-polyacrylamide gel electrophoresis with a pre-prepared 15% gel. Equal amounts of total protein (20 μg per lane) were loaded into the wells. The resolved proteins were transferred to a polyvinylidene difluoride membrane using a semi-dry transfer apparatus (Trans-Blot SD, Bio-Rad Laboratories, Hercules, CA, USA). The membrane was blocked with skim milk for 90 min to minimize non-specific binding and incubated with the following primary antibodies for 1 h: anti-TGFBR1 (ab235578, 1:1000, Abcam, Cambridge, MA, USA), anti-GDF11 (DF8364, 1:2000, Affinity, Cincinnati, OH, USA), anti-Smad2 (ab228765, 1:5000, Abcam, USA), anti-Smad2 (phospho S467) (ab280888, 1:1000, Abcam), Anti-Smad3 (AF6362, 1:1000, Affinity), anti-phospho-Smad3 (Ser423+Ser425) (AF8315, 1:2000, Affinity), anti-NFATc1 (66963-1-Ig, 1:50,000, Proteintech, Wuhan, China), anti-MMP9 (AF5228, 1:1000, Affinity), anti-c-Fos (66590-1-Ig, 1:30,000, Proteintech), anti-Cathepsin K (DF6614, 1:1000, Affinity), anti-IκB alpha (10268-1-AP, 1:20,000, Proteintech), anti-IκB alpha (phospho S36) (ab133462, 1:10,000, Abcam), anti-NF-κB p65 (AF5006, 1:1000, Affinity), and anti-GAPDH (AB0036, 1:5000, Abways, Shanghai, China). Next, the membrane was incubated with HRP-conjugated anti-rabbit IgG (711-035-152, 1:3000, Jackson ImmunoResearch, West Grove, PA, USA) or HRP-conjugated anti-mouse IgG (715-035-150, 1:5000, Jackson ImmunoResearch, West Grove, PA, USA). Immunoreactive signals were detected using SuperSignal reagents (34580, Pierce, Rockford, IL, USA). Densitometric analysis was performed using ImageJ software (1.48v). The levels of target proteins were normalized to those of the loading control.

2.9 Immunofluorescence Staining

The RAW264.7 cells after co-culture on the slides were rinsed, fixed with 4% paraformaldehyde for 30 min, permeabilized with 0.5% Triton X-100 at 37°C for 5 min to allow the penetration of antibodies into the cell compartments, and gently air-dried. Circles were drawn around the cells using a hydrophobic pen. The cells were then incubated with a blocking solution containing 5% FBS to reduce non-specific binding and incubated with anti-NFATC1 primary antibodies (DF6446, 1:200, Affinity) overnight at 4°C. Next, the cells were incubated with the secondary antibody (DyLight 594-conjugated AffiniPure goat anti-rabbit IgG (H+L), BA1142, 1:200, BOSTER, California, USA) for 1 h. The nuclei were counterstained with 4′,6-diamidino-2-phenylindole. Finally, an anti-fade mounting medium (P0131, Beyotime) was added to the slides before they were sealed. The cells were observed under a fluorescence microscope (IX73, Olympus, Tokyo, Japan). Images of five randomly selected fields were captured to analyze fluorescence intensity.

2.10 ELISA

The RAW264.7 cell culture supernatant was centrifuged at 2000× *g* for 20 min to sediment debris and cellular fragments. According to the instructions of the ELISA kit (E-EL-M0603, Elabscience, Wuhan, China), cells in each well were sequentially incubated with 100 μL of biotinylated antibody working solution at 37°C for 1 h and 100 μL of HRP-conjugated enzyme-labeled reagent at 37°C for 30 min. The samples were then incubated with a substrate solution in the dark at 37°C for 15 min. A standard curve was plotted based on the absorbance readings obtained from the standards. The expression of Gdf11 in the supernatant was quantified using the standard curve.

2.11 Statistical Analysis

All statistical analyses were performed using GraphPad Prism (ver. 6, San Diego, CA, USA). The data are presented as mean ± standard deviation. Means between two groups were compared using the two-tailed Student's *t*-test or the ratio paired *t*-test, while those between more than two groups were compared using one-way analysis of variance, followed by Tukey's post-hoc test. Differences were considered significant at $p < 0.05$.

3 Results

3.1 Bioinformatics Analysis of DEGs and Signaling Pathways in the MEC Dataset

The GSE116142 dataset was downloaded from the GEO database and subjected to bioinformatics analysis to identify the DEGs and signaling pathways. In total, 1406 significant DEGs (735 downregulated genes and 671 upregulated genes) were identified. Among the DEGs, the expression levels of *GDF11* and *TGFBR1* were significantly upregulated in MEC (Fig. 1A–C). Protein-protein interaction analysis using the STRING database revealed that GDF11 interacts with TGFBR1 (Fig. 1D). GO and KEGG functional enrichment analyses revealed that DEGs, including *GDF11* and *TGFBR1*, were enriched in SMAD protein signal transduction, cytokine-cytokine receptor interaction, and osteoclast differentiation (Fig. 1E,F). Furthermore, GSEA demonstrated that cytokine-cytokine receptor interaction and osteoclast differentiation pathways were enriched in MEC (Fig. 1G). These findings indicated that GDF11 and TGFBR1 in MEC may be related to SMAD signal transduction and osteoclast differentiation signaling pathways.

3.2 GDF11 and TGFBR1 Were Significantly Upregulated in MEC and Are Associated with Osteoclasts

The expression levels of GDF11 and TGFBR1 were further validated in MEC clinical samples. Immunohistochemical analysis demonstrated that the number of $GDF11^+$ and $TGFBR1^+$ cells in MEC samples was significantly higher than that in retroauricular skin samples (Fig. 2A). Western blotting analysis revealed that the GDF11, TGFBR1, and phosphorylated SMAD2/3 levels in MEC samples were significantly upregulated when compared with those in retroauricular skin samples (Fig. 2B). Furthermore, RT-qPCR analysis demonstrated that the mRNA levels of *GDF11*, *TGFBR1*, and osteoclast-related factors (*TRAP* and *NFATC1*) were significantly upregulated in MEC samples (Fig. 2C). These findings suggest that GDF11 and TGFBR1 are significantly upregulated in MEC and that they are associated with osteoclast differentiation.

3.3 Effect of Exogenous rGDF11 on the Differentiation of RAW264.7 Cells into Osteoclasts

The effects of different concentrations of rGDF11 on the differentiation of RAW264.7 cells into osteoclasts were examined. TRAP staining revealed that RAW264.7 cells treated with 50 ng/mL rGDF11 exhibited the highest number of $TRAP^+$ cells (Fig. 3A,B). RT-qPCR analysis revealed that the mRNA levels of *Trap* were the highest in macrophages treated with 50 ng/mL rGDF11 (Fig. 3C). Consistently, western blotting analysis demonstrated that 50 ng/mL rGDF11 upregulated the expression levels of Tgfbr1 and phosphorylated Smad2/3 in macrophages (Fig. 3D,E). Thus, subsequent experiments were performed using 50 ng/mL rGDF11 to induce RAW264.7 cell differentiation. However, treatment with AZ12601011 mitigated the rGDF11-induced differentiation of macrophages into $TRAP^+$ cells and upregulation of Trap, Tgfbr1, and phosphorylated Smad2/3. This suggests that rGDF11 promotes the differentiation of macrophages into osteoclasts and upregulates Tgfbr1 and phosphorylated Smad2/3. However, treatment with AZ12601011 mitigated the effects of rGDF11. Thus, exogenous rGDF11 promotes the differentiation of RAW264.7 cells into osteoclasts.

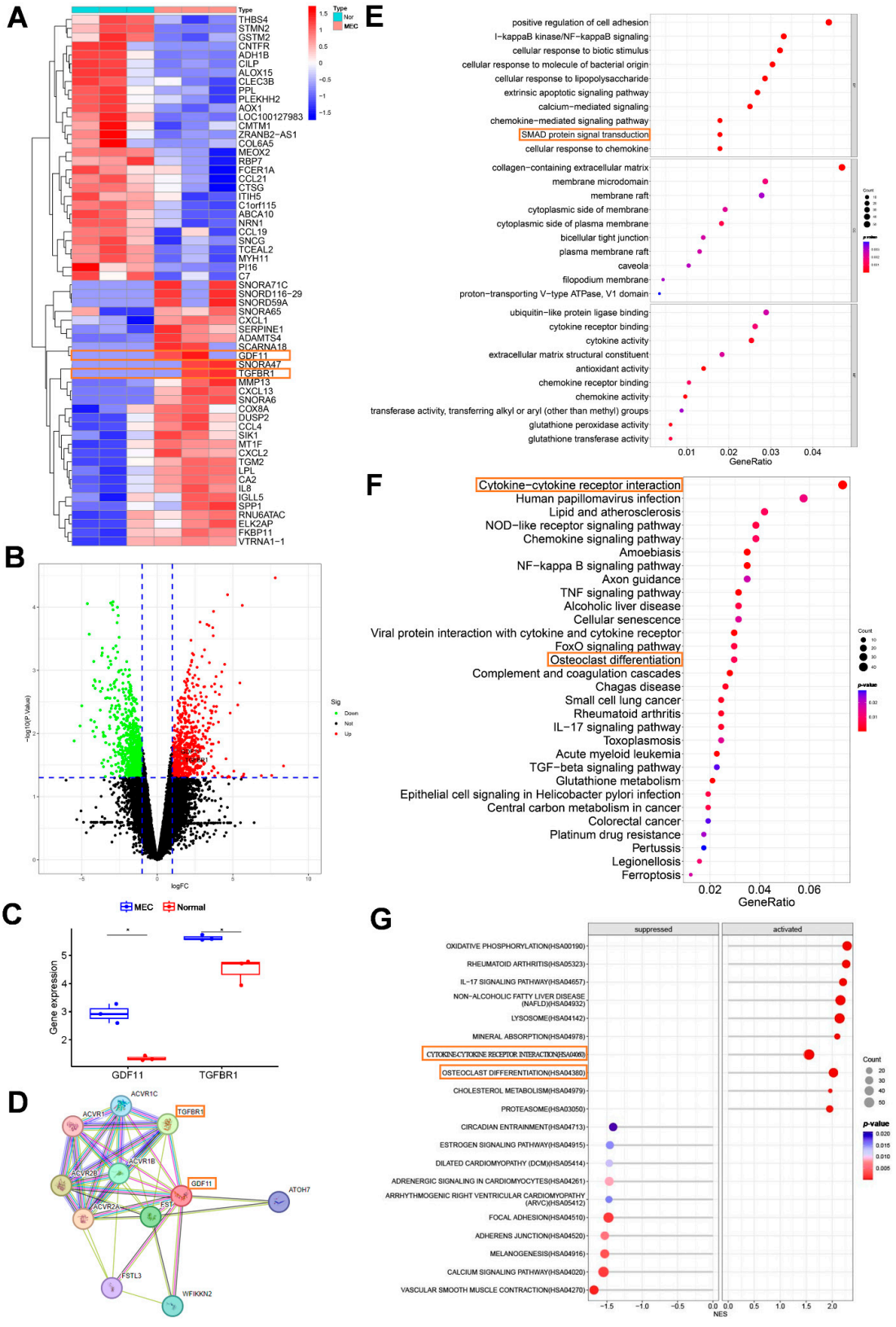

Figure 1: Bioinformatic analysis of the middle ear cholesteatoma (MEC) dataset (GSE116142). (**A**) Heatmap plot showing the top 30 upregulated genes and the top 30 downregulated genes in the GSE116142 dataset. (**B**) Differentially

expressed genes (DEGs) between retroauricular dermis and MEC samples are displayed in the volcano plot. The red and green dots indicate upregulated and downregulated genes, respectively. (**C**) Box plots displaying the differential expression levels of GDF11 and TGFBR1 between MEC and retroauricular dermis samples. $^{*}p < 0.05$. (**D**) STRING interactome network (https://string-db.org/cgi/input.pl) predicts the interaction between GDF11 and TGFBR1. (**E**,**F**) Gene Ontology and Kyoto Encyclopedia of Genes and Genomes functional enrichment analyses of DEGs. (**G**) Gene set enrichment analysis of DEGs.

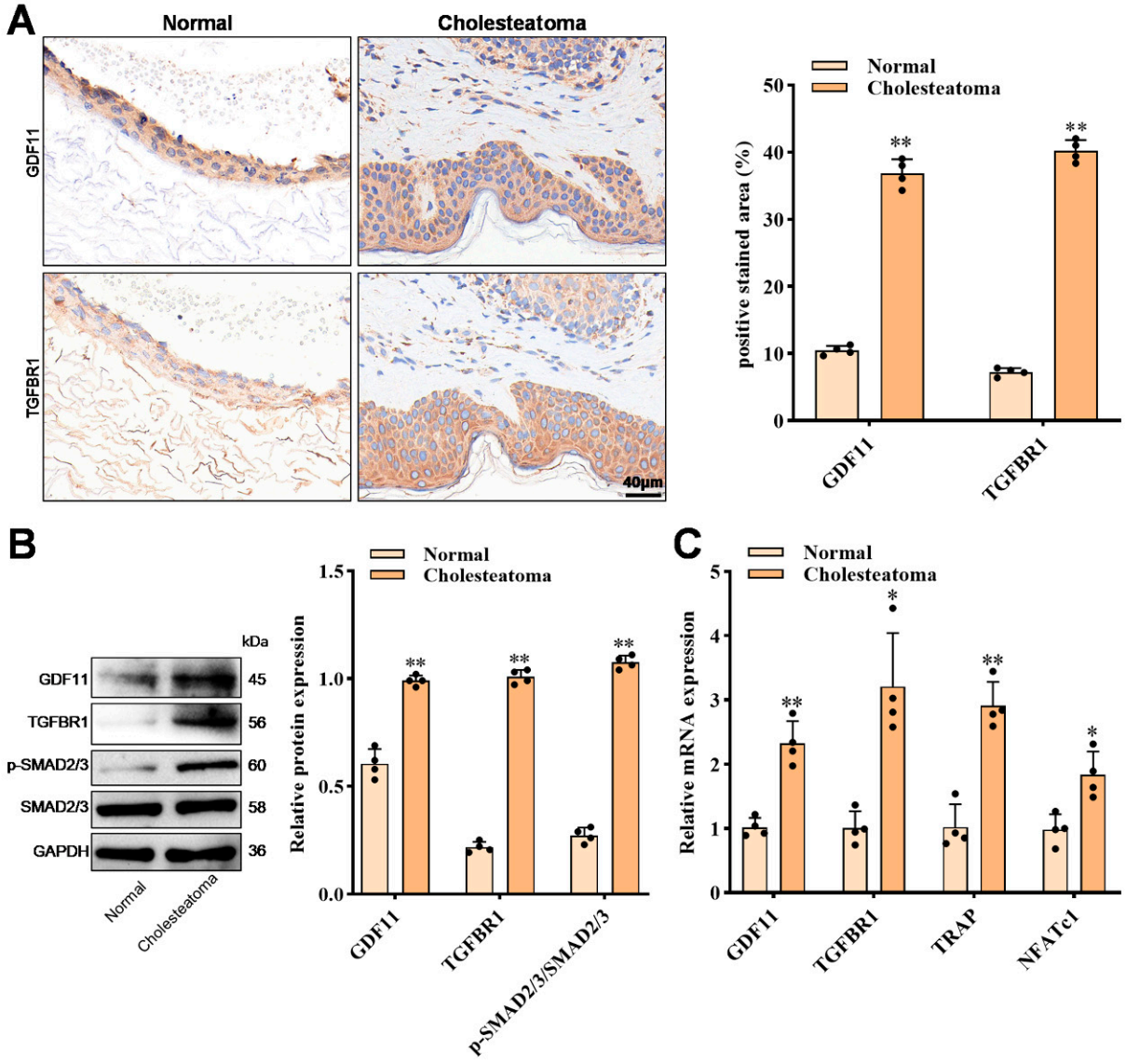

Figure 2: GDF11 and TGFBR1 are significantly upregulated in middle ear cholesteatoma (MEC). (**A**) The expression levels of GDF11 and TGFBR1 in MEC and retroauricular skin samples were evaluated using immunohistochemical analysis ($n = 4$). (**B**) Western blotting analysis of the expression levels of GDF11, TGFBR1, and SMAD2/3 in MEC and retroauricular skin samples ($n = 4$). (**C**) The mRNA expression levels of *GDF11*, *TGFBR1*, and osteoclast-related factors (*TRAP* and *NFATC1*) in MEC and retroauricular skin samples were assessed using quantitative real-time polymerase chain reaction analysis ($n = 4$). The mRNA expression levels of target genes were normalized to those of *GAPDH*. The expression levels were determined using the $2^{-\Delta\Delta Ct}$ method. Data are represented as mean ± standard deviation; $^{*}p < 0.05$, $^{**}p < 0.01$.

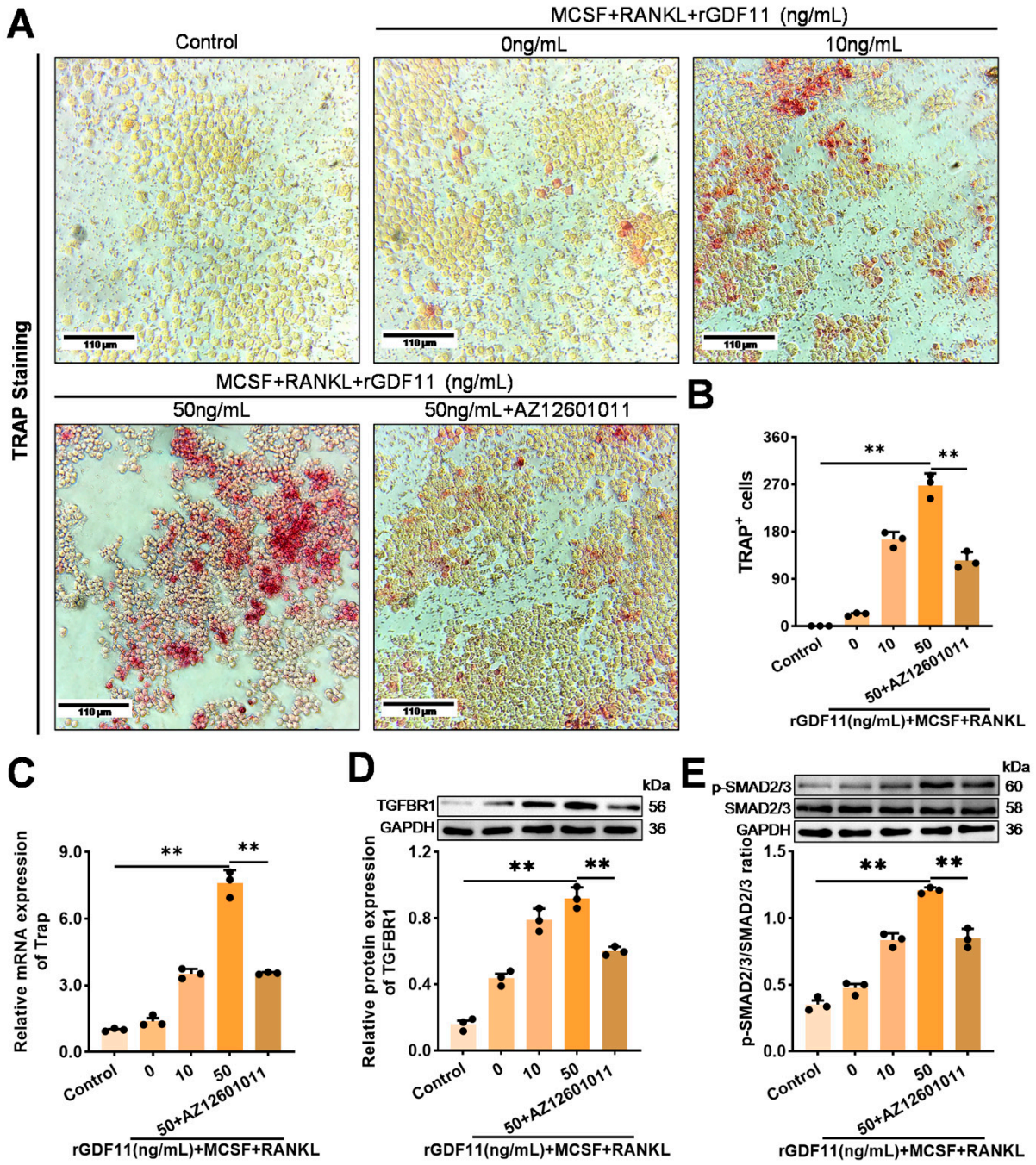

Figure 3: Effect of exogenous recombinant GDF11 (rGDF11) on the differentiation of macrophages into osteoclasts. Cells were treated with macrophage colony-stimulating factor (M-CSF) and receptor activator of nuclear factor-κB ligand (RANKL) to induce osteoclast differentiation. (**A**,**B**) The effect of exogenous rGDF11 on the differentiation of RAW264.7 cells into osteoclasts was evaluated using tartrate-resistant acid phosphatase (TRAP) staining; (**C**) The mRNA expression levels of *Trap* in RAW264.7 cells were determined using quantitative real-time polymerase chain reaction analysis. The expression levels of *Trap* were normalized to those of *Gapdh*. The relative expression levels were calculated using the $2^{-\Delta\Delta Ct}$ method; (**D**,**E**) Western blotting analysis of the expression of TGFBR1 and phosphorylated SMAD2/3 in RAW264.7 cells. Data are represented as mean ± standard deviation ($n = 3$). $^{**}p < 0.01$.

3.4 Exogenous rGDF11 Promotes the Expression of Differentiation-Related Markers in RAW264.7 Cells

Next, the effect of different concentrations of rGDF11 on the expression of markers associated with RAW264.7 cell differentiation into osteoclasts was examined. Immunofluorescence analysis revealed that Nfatc1 expression was upregulated in rGDF11-induced RAW264.7 cells (Fig. 4A). Furthermore, western blotting analysis revealed that rGDF11 upregulated the expression of osteoclast-related markers (c-Fos, NFATC1, CTSK, and MMP9) and the phosphorylation of IκB-α and p65 (Fig. 4B,C). This suggests that rGDF11 promotes the differentiation of macrophages into osteoclasts and upregulates osteoclast-related factors in RAW264.7 cells.

3.5 Fibroblasts Secrete GDF11 Protein to Promote the Differentiation of Macrophages into Osteoclasts

Recombinant fibroblast lines were established to overexpress or knock down *Gdf11* and co-cultured with macrophages. RT-qPCR and western blotting analyses revealed that transduction with the *Gdf11* overexpression construct upregulated the expression of GDF11, TGFBR1, and phosphorylated SMAD2/3 in fibroblasts (Fig. 5A–C). In contrast, shGDF11 transduction downregulated the expression of GDF11, TGFBR1, and phosphorylated SMAD2/3 (Fig. 5A–C).

Additionally, co-culturing GDF11 overexpression-transduced fibroblasts with macrophages increased the number of $TRAP^+$ cells (Fig. 5D,E), the secretion of Gdf11 in the macrophage culture medium (Fig. 5F), and the expression of Trap, Nfatc1, Gdf11, Tgfbr1, and phosphorylated Smad2/3 in macrophages (Fig. 5G–K). Consistently, co-culturing shGDF11-transduced fibroblasts decreased the number of $TRAP^+$ macrophages (Fig. 5D,E), the secretion of GDF11 in the macrophage culture medium (Fig. 5F), and the expression of *Trap*, NFATc1, GDF11, TGFBR1, and phosphorylated SMAD2/3 in macrophages (Fig. 5G–K). These findings indicated that fibroblasts promote the differentiation of macrophages into osteoclasts by secreting GDF11.

3.6 Gdf11 Secretion from Fibroblasts through the Tgfbr1/Smad2/3 Pathway Induces Macrophage Differentiation into Osteoclasts

RT-qPCR and western blotting analyses revealed that AZ12601011 did not affect the expression of Gdf11 but downregulated the expression of Tgfbr1 and phosphorylated Smad2/3 (Fig. 6A–C). Treatment of Gdf11-overexpressing fibroblasts with AZ12601011 did not alter the downregulated expression of Tgfbr1 and phosphorylated Smad2/3 (Fig. 6A–C).

AZ12601011-treated fibroblasts were co-cultured with RAW264.7 cells. TRAP staining analysis revealed that AZ12601011 decreased the number of $Trap^+$ cells (Fig. 6D,E). The ELISA results revealed that the concentration of secreted Gdf11 was downregulated in the culture medium of macrophages co-cultured with AZ12601011-treated fibroblasts (Fig. 6F). Additionally, the expression levels of Trap and Nfatc1 were downregulated in macrophages co-cultured with AZ12601011-treated fibroblasts (Fig. 6G,H). RT-qPCR and western blotting analyses indicated that the expression levels of Gdf11, Tgfbr1, and Smad2/3 were downregulated in macrophages co-cultured with AZ12601011-treated fibroblasts (Fig. 6I–K). Meanwhile, macrophages co-cultured with AZ12601011-treated Gdf11-overexpressing fibroblasts exhibited decreased differentiation into $Trap^+$ cells (Fig. 6D,E), secretion of Gdf11 in the macrophage culture medium (Fig. 6F), expression of Trap, Nfatc1 (Fig. 6G,H), Gdf11, Tgfbr1 (Fig. 6I,J), and phosphorylated Smad2/3 (Fig. 6K,L). This effect was similar to that in the AZ12601011-treated group. These results indicate that GDF11 in fibroblasts targets TGFBR1, promotes the phosphorylation of SMAD2/3 and the secretion of GDF11, upregulates the expression of GDF11 in macrophages, and induces macrophage differentiation into osteoclasts through the TGFBR1/SMAD2/3 pathway.

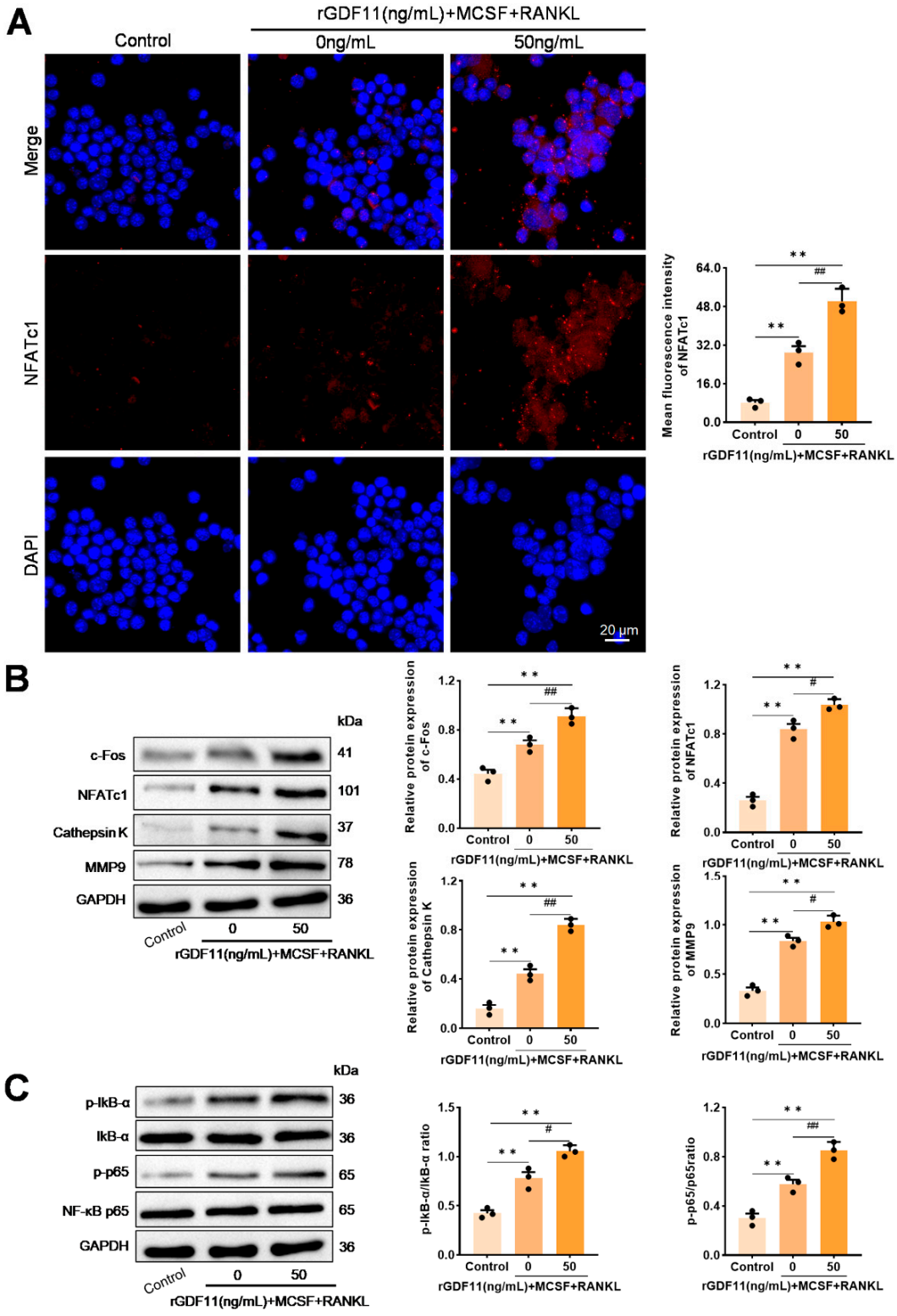

Figure 4: Effect of exogenous recombinant GDF11 (rGDF11) on the expression of markers related to RAW264.7 cell differentiation into osteoclasts. Cells were treated with macrophage colony-stimulating factor (M-CSF) and receptor activator of nuclear factor-κB ligand (RANKL) to induce osteoclast differentiation. (**A**) Nfatc1 expression in RAW264.7 cells was determined using immunofluorescence staining; (**B**) Western blotting analysis of the expression of osteoclast-related

indicators (c-Fos, NFATC1, CTSK, and MMP9) in RAW264.7 cells; (**C**) Western blotting analysis of the expression of phosphorylated IκB-α and p65 in RAW264.7 cells. Data are represented as mean ± standard deviation ($n = 3$). $^{**}p < 0.01$, compared with the control group; $^{\#}p < 0.05$, $^{\#\#}p < 0.01$, compared with the 0 ng/mL rGDF11 + M-CSF + RANKL group.

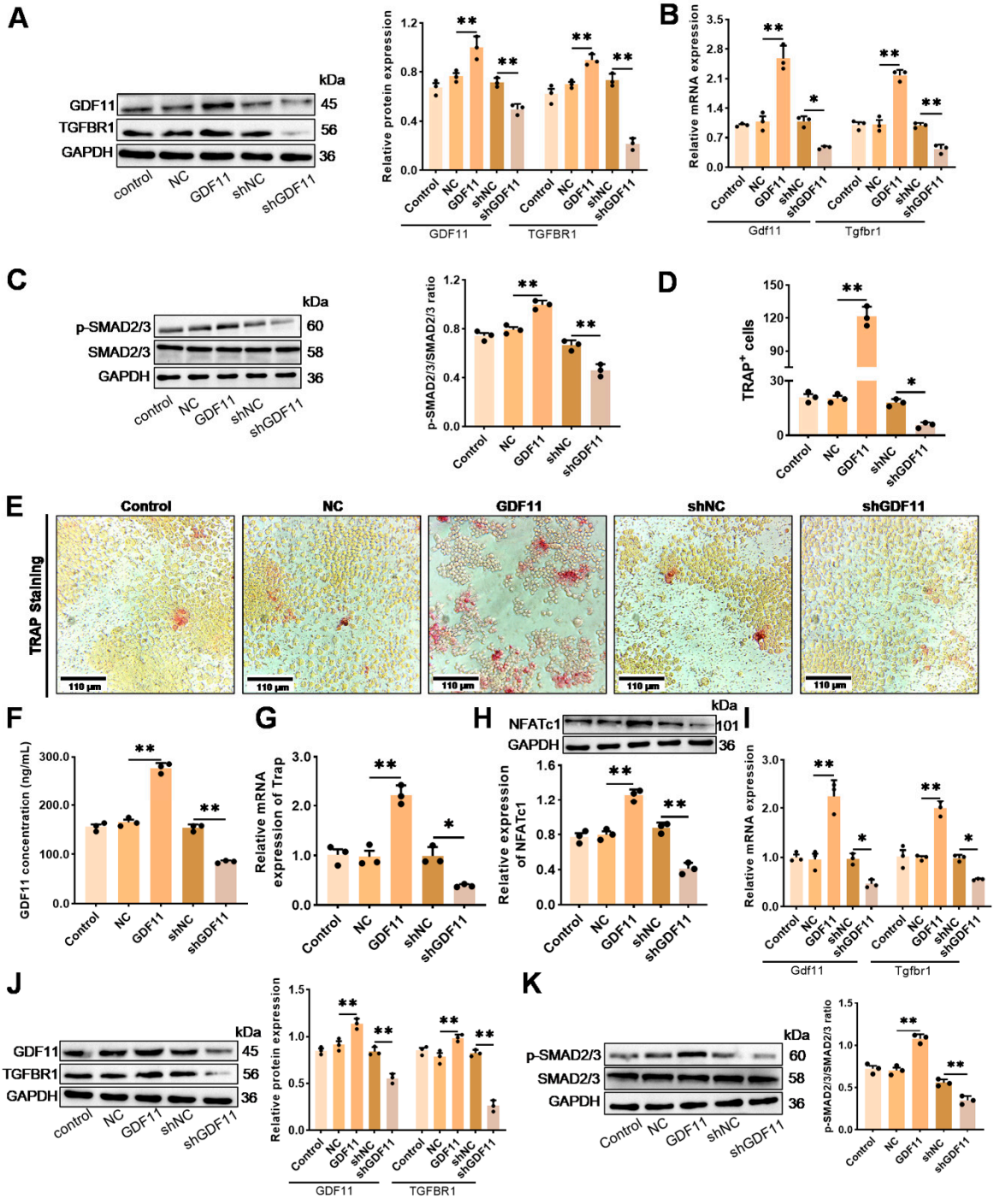

Figure 5: Effect of fibroblast-derived GDF11 on the differentiation of macrophages into osteoclasts. (**A**,**B**) Gdf11 and Tgfbr1 expression levels in NIH-3T3 cells were assessed using quantitative real-time polymerase chain reaction (RT-qPCR) and western blotting analyses; (**C**) The expression of phosphorylated Smad2/3 in NIH-3T3 cells was assessed using western blotting analysis; (**D**,**E**) Tartarate-resistant acid phosphatase (TRAP) staining was performed

to assess the effect of co-culturing NIH-3T3 cells with RAW264.7 cells on osteoclast differentiation. (**F**) The concentration of Gdf11 in the co-culture medium was examined using the enzyme-linked immunosorbent assay. (**G**) The mRNA expression of *TRAP* in co-cultured RAW264.7 cells was examined using RT-qPCR analysis; (**H**) The expression of Nfatc1 in co-cultured RAW264.7 cells was assessed using western blotting; (**I**,**J**) The mRNA expression levels of *Gdf11* and *Tgfbr1* in RAW264.7 cells were assessed using RT-qPCR and western blotting analyses; (**K**) Western blotting analysis of the expression of phosphorylated Smad2/3 in co-cultured RAW264.7 cells. Control group: co-culture of untreated NIH-3T3 cells with RAW264.7 cells. The relative expression levels of target genes were normalized to those of *Gapdh*. The relative expression levels were determined using the $2^{-\Delta\Delta Ct}$ method. Data are represented as mean ± standard deviation (n = 3). $^{*}p < 0.05$, $^{**}p < 0.01$.

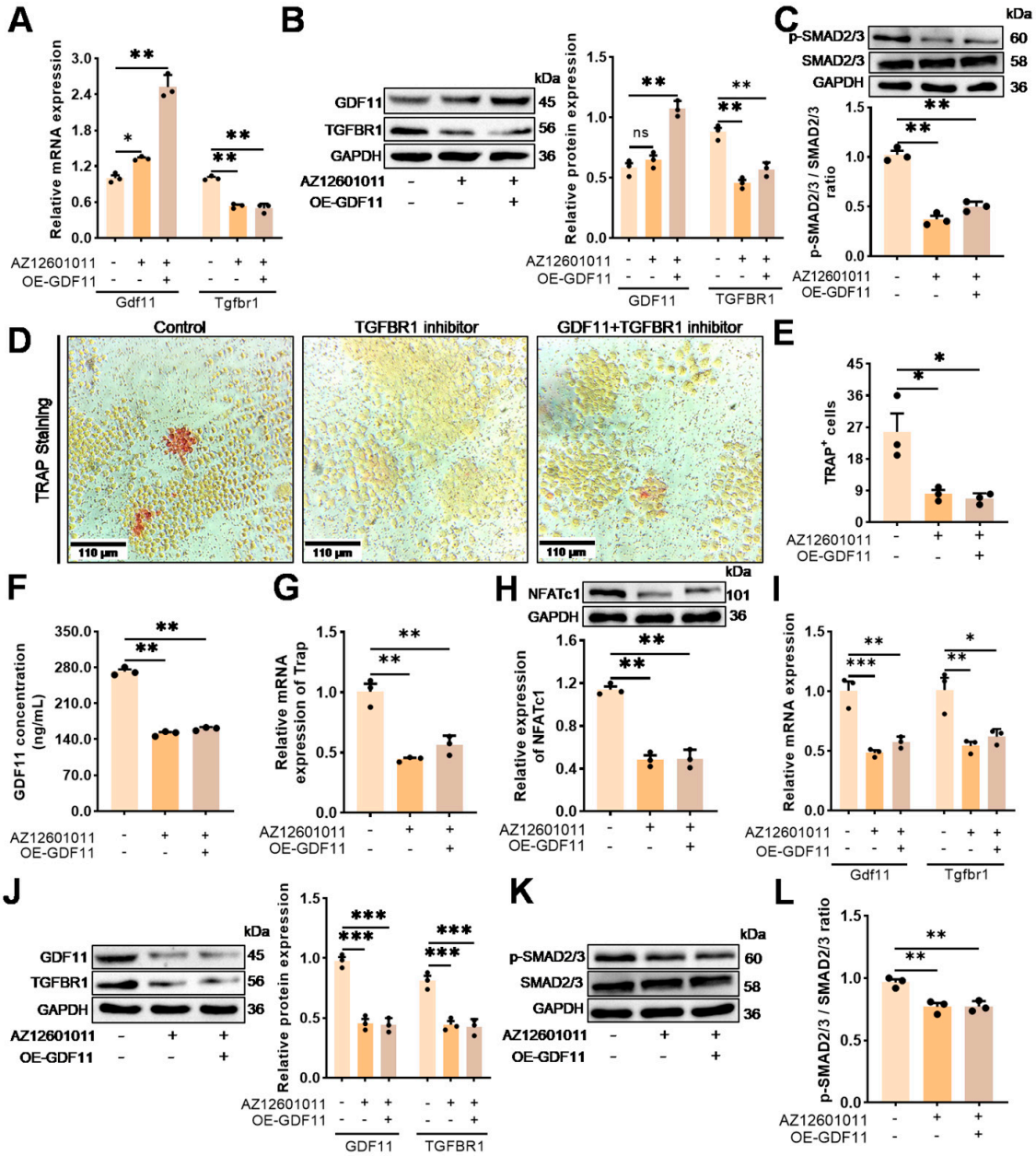

Figure 6: NIH-3T3-derived Gdf11 targeted the Tgfbr1/Smad2/3 axis to promote Gdf11 secretion and the differentiation of RAW264.7 cells into osteoclasts. (**A**,**B**) The expression levels of Gdf11 and Tgfbr1 in NIH-3T3 cells were assessed

using quantitative real-time polymerase chain reaction and western blotting analyses. (**C**) The relative level of phosphorylated Smad2/3 in NIH-3T3 cells was assessed using western blotting analysis. (**D**,**E**) Tartrate-resistant acid phosphatase (TRAP) staining was performed to examine the effect of co-culturing NIH-3T3 with RAW264.7 cells on osteoclast differentiation. (**F**) The concentration of Gdf11 in the co-culture medium was examined using the enzyme-linked immunosorbent assay. (**G**) The mRNA levels of *TRAP* in co-cultured RAW264.7 cells were examined using RT-qPCR analysis; (**H**) The expression of Nfatc1 in co-cultured RAW264.7 cells was assessed using western blotting analysis; (**I**,**J**) The expression levels of Gdf11 and Tgfbr1 in RAW264.7 cells were assessed using RT-qPCR and western blotting analyses. (**K**,**L**) Western blotting analysis of the expression of phosphorylated Smad2/3 in co-cultured RAW264.7 cells. Control group: co-culture of untreated NIH-3T3 cells with RAW264.7 cells. The expression levels of target genes were normalized to those of *Gapdh*. The relative expression levels were calculated using the $2^{-\Delta\Delta Ct}$ method. Data are represented as mean ± standard deviation (n = 3). $^{*}p < 0.05$, $^{**}p < 0.01$, $^{***}p < 0.001$; ns, not significant.

4 Discussion

Acquired cholesteatoma, which typically emerges with a history of primary or secondary otitis media, manifests as a chronic inflammatory condition characterized by tympanic membrane perforation or retraction pocket and bone destruction [25]. The etiological factors for bone erosion in human cholesteatoma include pressure necrosis, collagenolytic enzymes, TNF-α, lysosomal enzymes, and non-lysosomal enzymes (calpain I and II) [26]. The role of osteoclast-mediated bone resorption in cholesteatoma pathogenesis has piqued the interest of the scientific community. The proliferation and maturation of osteoclasts directly affect the severity of bone resorption in cholesteatoma-induced middle ear damage [22]. The findings of this study indicate that GDF11 promotes RANKL-dependent osteoclast differentiation by activating the SMAD2/3 signaling pathway via TGFBR1. Furthermore, analysis using an *in vitro* co-culture system of fibroblasts and macrophages revealed that fibroblasts promoted osteoclast differentiation in macrophages through the paracrine activity of secreted GDF11.

Osteoclast formation, a multi-stage process, is regulated by various genetic, humoral, and mechanical factors [27]. Transcriptomic and clinical sample analyses demonstrated that GDF11 and TGFBR1 were upregulated in cholesteatoma perimatrix and MEC samples. GDF11 is reported to impede osteoblast differentiation and stimulate RANK-induced osteoclast formation through NFATC1 stimulation via the SMAD2/3 and c-FOS pathways [17,19]. Treatment with a GDF11 inhibitor effectively attenuates bone loss in mouse models [28]. Additionally, GDF11 is closely associated with bone resorption in periodontal disease [29]. Treatment with GDF11 alone does not enhance osteoclastogenic potential in bone marrow-derived macrophages [17]. Therefore, this study investigated the role and mechanism of Gdf11 in the presence of Rankl. Gdf11 promoted the osteoclastic differentiation of RAW264.7 cells as evidenced by an increase in the number of $Trap^{+}$ cells and the upregulation of Fos, Nfatc1, Ctsk, and Mmp9. FOS/NFATC1 is a critical transcription factor involved in osteoclast differentiation, playing a pivotal role in osteoclast formation and bone resorption [30,31]. The DNA binding of c-Fos is dependent on SMAD2/3. FOS and SMAD2/3 cooperatively regulate the expression of NFATC1 and the RANKL-induced generation of osteoclasts [32]. NFATC1 subsequently activates multiple osteoclast-specific genes, including those encoding CTSK, TRAP, and MMP9 [33–35]. TRAP is an established osteoclast marker and is correlated with bone resorption activity [36]. Additionally, the phosphorylation of RELA and NFKNIA is closely associated with the activation of the canonical RANKL signaling pathway [37,38]. NF-κB regulates various cellular and organismal processes by promoting *NFATC1* transcription [39,40]. GDF11 may synergistically enhance NFATC1 transcription through the SMAD2/3 and NF-κB pathways [38]. This study demonstrated that

treatment with GDF11 significantly upregulated the expression levels of these key effector molecules. Thus, the GDF11 and RANK signaling pathways exert synergistic effects to promote osteoclast differentiation.

Furthermore, the TGFBR1-SMAD2/3 pathway was a critical downstream mechanism through which GDF11 promoted osteoclast differentiation. In both cholesteatoma stroma and MEC samples, the expression levels of TGFBR1 and phosphorylated SMAD2/3 were upregulated. Similar to other members of the TGF-β superfamily, GDF11 transmits signals through type I (e.g., ACVR2B, ACVR2B) and type II (e.g., ALK4, ALK5, ALK7) serine/threonine kinase receptors, promoting the phosphorylation of SMAD2/3 [41,42]. TGFBR1 (ALK5) plays a crucial role in the signal transduction of GDF11 [43]. Experiments with AZ12601011 confirmed that Gdf11 promoted Smad2/3-mediated osteoclastogenesis through Tgfbr1 in RAW264.7 cells. However, the potential effect of AZ12601011 cannot be ruled out. In addition to the canonical signaling pathways, GDF11 also induces other signaling cascades, including MAP kinases (p38, ERK, and JNK) and PI3K/AKT [41,44]. The potential roles of these pathways in MEC must be further explored.

Fibroblasts, a crucial component of the stroma in MEC, in combination with macrophages, play important roles in bone erosion. Histological studies have revealed the aggregation of fibroblasts and macrophages in the subepithelial region, which is accompanied by increased capillary proliferation [5]. Additionally, single-cell RNA sequencing of human cholesteatoma specimens revealed the presence of a specific pathogenic fibroblast subpopulation expressing upregulated levels of INHBA (inhibin βA) in the stromal microenvironment of cholesteatoma. This subpopulation promotes the expression of activin A for RANKL-dependent osteoclastogenesis [45]. These findings suggest that the crosstalk between fibroblasts and monocytes/macrophages may play a crucial role in the local regulation of osteoclast activation and MEC recruitment, although the underlying mechanisms are unclear. In this study, an *in vitro* co-culture system was constructed to study the mechanisms of interaction between these two cell types. The modulation of Gdf11 expression levels in fibroblasts revealed that the secretion of Gdf11 by fibroblasts significantly affects the osteoclast differentiation of RAW264.7 cells. These findings suggested that fibroblasts may promote RANKL-dependent osteoclastogenesis by secreting GDF11, which activates the TGFBR1-SMAD2/3 signaling pathway in macrophages through a paracrine mechanism.

In fibroblasts, the paracrine effects of GDF11 influence surrounding cells (such as cardiomyocytes and vascular endothelial cells), regulating their proliferation, migration, and extracellular matrix synthesis through autocrine effects [46]. In this study, the expression of Gdf11 significantly affected the activation of the Smad2/3 axis in fibroblasts. AZ12601011 did not affect the Gdf11 expression levels in fibroblasts but significantly inhibited its secretion. Thus, AZ12601011 impaired the ability of Gdf11-overexpressing fibroblasts to induce osteoclast differentiation. TGF-β family ligands can self-regulate their transcription by activating the Smad signaling pathway [47]. Fibroblasts are associated with an autocrine positive feedback loop involving GDF11 and TGFBR1 that enhances the transcription and secretion of GDF11. This dual regulatory mechanism can form a sustained, GDF11-mediated amplification loop of pro-osteoclastogenic signals within the cholesteatoma microenvironment (Fig. 7).

This study is associated with several limitations. A limited sample size and the lack of representative samples may affect the generalizability and reliability of the results. This study demonstrated that GDF11 and TGFBR1 are upregulated in MEC and are associated with SMAD signaling and osteoclast differentiation. However, further studies are needed to investigate the specific regulatory mechanisms of these molecules. In addition to the SMAD2/3 signaling pathway, other non-canonical pathways (e.g., MAPK/PI3K) must be explored. Furthermore, the effects of rGDF11 on osteoclast differentiation were analyzed using *in vitro* experiments with the RAW264.7 cell line. However, these findings were not validated *in vivo*. Establishing animal models is crucial to verify the relationship between GDF11 and osteoclast differentiation. This study

did not investigate the safety of GDF11 and TGFBR1 inhibitors on auditory function. The TGFBR1 inhibitor AZ12601011 inhibits osteoclast differentiation. However, further studies are needed to determine the selectivity and potential side effects of AZ12601011 and evaluate its practical feasibility as a therapeutic. Finally, this study analyzed osteoclast differentiation markers but did not perform a functional bone resorption assay. Therefore, whether these differentiated cells possess active bone-resorbing capacity remains to be validated. Future studies incorporating functional resorption assays are necessary to confirm this activity.

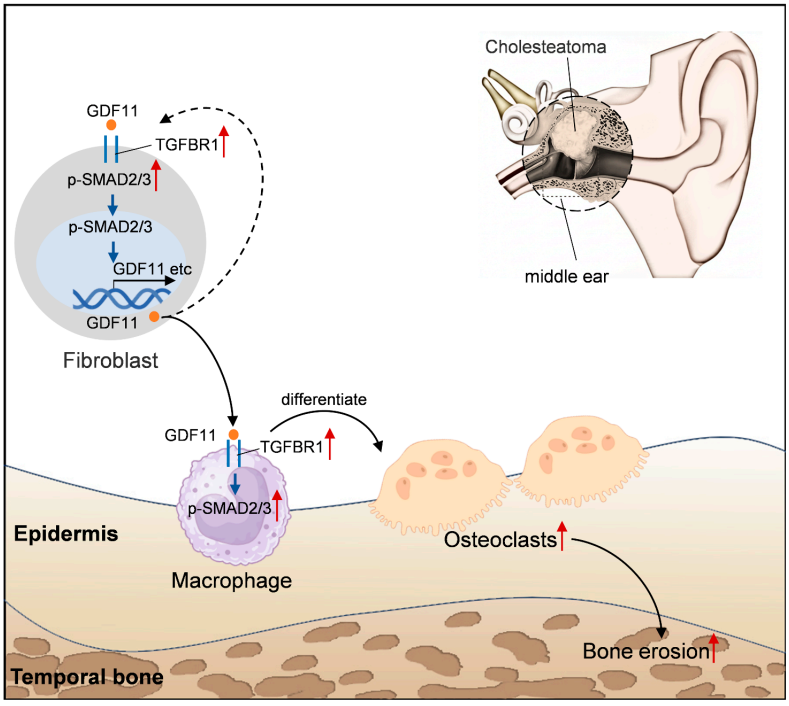

Figure 7: Fibroblasts secrete GDF11 protein to promote osteoclast differentiation in middle ear cholesteatoma (MEC) through the TGFBR1-mediated SMAD2/3 pathway. Red upward arrows indicate upregulation. Solid black arrows indicate direct promotion or differentiation. Dashed black arrows indicate a hypothetical or indirect mechanism. Some of the graphical elements were generated using Nano Banana (https://gemini.google.com/app), and other elements were drawn using Adobe Photoshop CS6 Extended (Version 13.0 ×64, Adobe Systems Incorporated, San Jose, CA, USA).

5 Conclusions

GDF11 upregulation in fibroblasts may promote secretion of GDF11 via the TGFBR1/SMAD2/3 signaling pathway. This resulted in the upregulation of GDF11 in macrophages. GDF11 promotes the differentiation of macrophages into osteoclasts by targeting TGFBR1 through the upregulation of phosphorylated SMAD2/3 levels. Analysis of the intercellular communication mechanisms between fibroblasts and macrophages that influence the differentiation and functionality of osteoclasts can offer valuable insights for developing therapeutic strategies for cholesteatoma-induced bone erosion and non-surgical treatment for cholesteatoma.

Acknowledgement: None.

Funding Statement: This work was supported by Natural Science Foundation of Ningxia Province (Grant No.: 2022AAC03521).

Author Contributions: The authors confirm contribution to the paper as follows: study conception and design: Xiaoping Gao; data collection: Zhikai Wang and Xing Wang; analysis and interpretation of results: Zhikai Wang

and Xing Wang, Lun Dong, and Wei Wang; draft manuscript preparation: Zhikai Wang and Xing Wang. All authors reviewed and approved the final version of the manuscript.

Availability of Data and Materials: The datasets used and/or analysed during the current study are available from the corresponding author on reasonable request.

Ethics Approval: This study was approved by the Medical Research Ethics Review Committee of the General Hospital of Ningxia Medical University (Approval No.: KYLL-2021-612) in accordance with the Declaration of Helsinki. Written informed consent was obtained from the patients.

Conflicts of Interest: The authors declare no conflicts of interest.

Appendix A

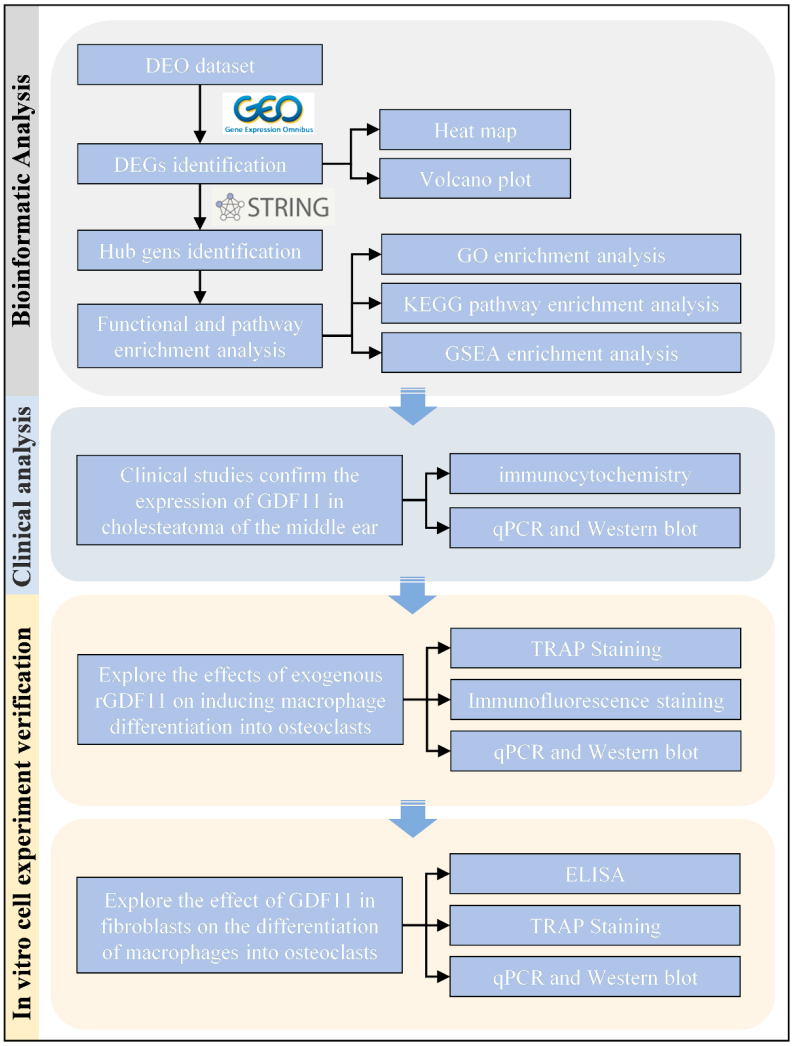

Figure A1: Study flowchart. The large blue downward arrows indicate the progression of the experimental phases (from top to bottom). The small black arrows indicate specific analytical methods or parallel detection techniques derived from the main steps. The graphical elements were assembled and labeled using Adobe Photoshop CS6 Extended (Version 13.0 x64, Adobe Systems Incorporated, San Jose, CA, USA).

Table A1: Clinical characteristics of patients with acquired middle ear cholesteatoma.

No.	Age	Sex	Disease Duration	Cholesteatoma Type
1	69	Female	8 months	Acquired MEC
2	41	Female	4 years	Acquired MEC
3	29	Male	19 years	Acquired MEC
4	56	Female	6 months	Acquired MEC
5	21	Female	2 years	Acquired MEC
6	39	Male	1 years	Acquired MEC
7	61	Male	10 years	Acquired MEC
8	55	Male	2 years	Acquired MEC

References

1. Imai R, Sato T, Iwamoto Y, Hanada Y, Terao M, Ohta Y, et al. Osteoclasts modulate bone erosion in cholesteatoma via RANKL signaling. J Assoc Res Otolaryngol. 2019;20(5):449–59. [CrossRef].
2. Satoh C, Yoshiura KI, Mishima H, Yoshida H, Takahashi H, Kumai Y. Proto-oncogene mutations in middle ear cholesteatoma contribute to its pathogenesis. BMC Med Genom. 2023;16(1):288. [CrossRef].
3. Schurmann M, Goon P, Sudhoff H. Review of potential medical treatments for middle ear cholesteatoma. Cell Commun Signal. 2022;20(1):148. [CrossRef].
4. Samara P, Athanasopoulos M, Athanasopoulos I. Benign, persistent, and invasive: Mechanistic and translational approaches to middle-ear cholesteatoma. Explor Target Anti-Tumor Ther. 2026;7:1002359. [CrossRef].
5. Chole RA. Osteoclasts in chronic otitis media, cholesteatoma, and otosclerosis. Ann Otol Rhinol Laryngol. 1988;97(6 Pt 1):661–6.
6. Delsmann MM, Bonik P, Ocokoljic A, Haussler SM, Puschel K, Praetorius M, et al. Cholesteatoma severely impacts the integrity and bone material quality of the incus. Calcif Tissue Int. 2023;113(6):609–17. [CrossRef].
7. De Leon-Oliva D, Barrena-Blazquez S, Jimenez-Alvarez L, Fraile-Martinez O, Garcia-Montero C, Lopez-Gonzalez L, et al. The RANK-RANKL-OPG system: A multifaceted regulator of homeostasis, immunity, and cancer. Medicina. 2023;59(10):1752. [CrossRef].
8. Ma Y, Shi X, Zhao H, Song R, Zou H, Zhu J, et al. Potential mechanisms of osteoprotegerin-induced damage to osteoclast adhesion structures via P2X7R-mediated MAPK signaling. Int J Mol Med. 2022;49(5):59. [CrossRef].
9. Sun B, Wu H, Lu J, Zhang R, Shen X, Gu Y, et al. Irisin reduces bone fracture by facilitating osteogenesis and antagonizing TGF-beta/Smad signaling in a growing mouse model of osteogenesis imperfecta. J Orthop Translat. 2023;38:175–89. [CrossRef].
10. Nickel J, Mueller TD. Specification of BMP signaling. Cells. 2019;8(12):1579. [CrossRef].
11. Machelak W, Szczepaniak A, Jacenik D, Zielińska M. The role of GDF11 during inflammation—An overview. Life Sci. 2023;322:121650. [CrossRef].
12. Frohlich J, Kovacovicova K, Raffaele M, Virglova T, Cizkova E, Kucera J, et al. GDF11 inhibits adipogenesis and improves mature adipocytes metabolic function via WNT/β-catenin and ALK5/SMAD2/3 pathways. Cell Prolif. 2022;55(10):e13310. [CrossRef].
13. Wang Z, Jiang P, Liu F, Du X, Ma L, Ye S, et al. GDF11 regulates PC12 neural stem cells via ALK5-dependent PI3K-Akt signaling pathway. Int J Mol Sci. 2022;23(20):12279. [CrossRef].
14. Wang H, Shi Y, He F, Ye T, Yu S, Miao H, et al. GDF11 inhibits abnormal adipogenesis of condylar chondrocytes in temporomandibular joint osteoarthritis. Bone Joint Res. 2022;11(7):453–64. [CrossRef].
15. Król W, Machelak W, Zielińska M. GDF11 as a friend or an enemy in the cancer biology? Biochim Biophys Acta Rev Cancer. 2023;1878(5):188944. [CrossRef].
16. Zhang Y, Shao J, Wang Z, Yang T, Liu S, Liu Y, et al. Growth differentiation factor 11 is a protective factor for osteoblastogenesis by targeting PPARgamma. Gene. 2015;557(2):209–14. [CrossRef].
17. Liu W, Zhou L, Zhou C, Zhang S, Jing J, Xie L, et al. GDF11 decreases bone mass by stimulating osteoclastogenesis and inhibiting osteoblast differentiation. Nat Commun. 2016;7:12794. [CrossRef].

18. Shen GS, Zhou HB, Zhang H, Chen B, Liu ZP, Yuan Y, et al. The GDF11-FTO-PPARγ axis controls the shift of osteoporotic MSC fate to adipocyte and inhibits bone formation during osteoporosis. Biochim Biophys Acta Mol Basis Dis. 2018;1864(12):3644–54. [CrossRef].
19. Lu Q, Tu ML, Li CJ, Zhang L, Jiang TJ, Liu T, et al. GDF11 Inhibits bone formation by activating Smad2/3 in bone marrow mesenchymal stem cells. Calcif Tissue Int. 2016;99(5):500–9. [CrossRef].
20. Liu X, Deng X, Ding R, Cheng X, Jia J. Chondrocyte suppression is mediated by miR-129-5p via GDF11/SMAD3 signaling in developmental dysplasia of the hip. J Orthop Res. 2020;38(12):2559–72. [CrossRef].
21. Iwamoto Y, Nishikawa K, Imai R, Furuya M, Uenaka M, Ohta Y, et al. Intercellular communication between keratinocytes and fibroblasts induces local osteoclast differentiation: A mechanism underlying cholesteatoma-induced bone destruction. Mol Cell Biol. 2016;36(11):1610–20. [CrossRef].
22. Gong N, Zhu W, Xu R, Teng Z, Deng C, Zhou H, et al. Keratinocytes-derived exosomal miRNA regulates osteoclast differentiation in middle ear cholesteatoma. Biochem Biophys Res Commun. 2020;525(2):341–7. [CrossRef].
23. Kuo CL. Etiopathogenesis of acquired cholesteatoma: Prominent theories and recent advances in biomolecular research. Laryngoscope. 2015;125(1):234–40. [CrossRef].
24. Spender LC, Ferguson GJ, Hughes GD, Davies BR, Goldberg FW, Herrera B, et al. Preclinical evaluation of AZ12601011 and AZ12799734, inhibitors of transforming growth factor β superfamily type 1 receptors. Mol Pharmacol. 2019;95(2):222–34. [CrossRef].
25. Wang S, Xie L, Zhang Y, Xu P, Liu A. Expression of prostaglandin E_2 receptors in acquired middle ear cholesteatoma. Clin Exp Otorhinolaryngol. 2018;11(1):17–22. [CrossRef].
26. Banerjee S, Mandal S, Sengupta A, Biswas KD, Basak B, Sengupta A, et al. A study on the correlation between preoperative radiological findings and intraoperative findings in cases of squamosal chronic otitis media. Eur J Cardiovasc Med. 2023;13(2):706–12.
27. Jin H, Yao L, Chen K, Liu Y, Wang Q, Wang Z, et al. Evodiamine inhibits RANKL-induced osteoclastogenesis and prevents ovariectomy-induced bone loss in mice. J Cell Mol Med. 2019;23(1):522–34. [CrossRef].
28. Jin Q, Qiao C, Li J, Xiao B, Li J, Xiao X. A GDF11/myostatin inhibitor, GDF11 propeptide-Fc, increases skeletal muscle mass and improves muscle strength in dystrophic mdx mice. Skelet Muscle. 2019;9(1):16. [CrossRef].
29. Li Y, Messina C, Bendaoud M, Fine DH, Schreiner H, Tsiagbe VK. Adaptive immune response in osteoclastic bone resorption induced by orally administered Aggregatibacter actinomycetemcomitans in a rat model of periodontal disease. Mol Oral Microbiol. 2010;25(4):275–92. [CrossRef].
30. Zhang Y, Yang M, Zhang S, Yang Z, Zhu Y, Wang Y, et al. BHLHE40 promotes osteoclastogenesis and abnormal bone resorption via c-Fos/NFATc1. Cell Biosci. 2022;12(1):70. [CrossRef].
31. Jeong B-C, Kim JH, Kim K, Kim I, Seong S, Kim N. ATF3 modulates calcium signaling in osteoclast differentiation and activity by associating with c-Fos and NFATc1 proteins. Bone. 2017;95:33–40. [CrossRef].
32. Omata Y, Yasui T, Hirose J, Izawa N, Imai Y, Matsumoto T, et al. Genomewide comprehensive analysis reveals critical cooperation between Smad and c-Fos in RANKL-induced osteoclastogenesis. J Bone Miner Res. 2015;30(5):869–77. [CrossRef].
33. Kim K, Punj V, Kim JM, Lee S, Ulmer TS, Lu W, et al. MMP-9 facilitates selective proteolysis of the histone H3 tail at genes necessary for proficient osteoclastogenesis. Genes Dev. 2016;30(2):208–19. [CrossRef].
34. Sundaram K, Nishimura R, Senn J, Youssef RF, London SD, Reddy SV. RANK ligand signaling modulates the matrix metalloproteinase-9 gene expression during osteoclast differentiation. Exp Cell Res. 2007;313(1):168–78. [CrossRef].
35. Takayanagi H. Osteoimmunology: Shared mechanisms and crosstalk between the immune and bone systems. Nat Rev Immunol. 2007;7(4):292–304. [CrossRef].
36. Rathod B, Desai S, Samvelyan HJ, Bock L, Wu J, Ohlsson C, et al. Tartrate-resistant acid phosphatase (TRAP/ACP5) promotes bone length, regulates cortical and trabecular bone mass, and maintains growth plate architecture and width in a sex- and site-specific manner in mice. Bone. 2024;188:117223. [CrossRef].
37. Chen XW, Liu WT, Wang YX, Chen WJ, Li HY, Chen YH, et al. Cyclopropanyldehydrocostunolide LJ attenuates high glucose-induced podocyte injury by suppressing RANKL/RANK-mediated NF-kappaB and MAPK signaling pathways. J Diabetes Complicat. 2016;30(5):760–9. [CrossRef].
38. Kajita T, Ariyoshi W, Okinaga T, Mitsugi S, Tominaga K, Nishihara T. Mechanisms involved in enhancement of osteoclast formation by activin-A. J Cell Biochem. 2018;119(8):6974–85. [CrossRef].

39. Boyce BF, Xiu Y, Li J, Xing L, Yao Z. NF-κB-mediated regulation of osteoclastogenesis. Endocrinol Metab. 2015;30(1):35–44. [CrossRef].
40. Oeckinghaus A, Hayden MS, Ghosh S. Crosstalk in NF-κB signaling pathways. Nat Immunol. 2011;12(8):695–708. [CrossRef].
41. Walker RG, Czepnik M, Goebel EJ, McCoy JC, Vujic A, Cho M, et al. Structural basis for potency differences between GDF8 and GDF11. BMC Biol. 2017;15(1):19. [CrossRef].
42. Zhang Y, Wei Y, Liu D, Liu F, Li X, Pan L, et al. Role of growth differentiation factor 11 in development, physiology and disease. Oncotarget. 2017;8(46):81604–16. [CrossRef].
43. Andersson O, Reissmann E, Ibanez CF. Growth differentiation factor 11 signals through the transforming growth factor-beta receptor ALK5 to regionalize the anterior-posterior axis. EMBO Rep. 2006;7(8):831–7. [CrossRef].
44. Walker RG, Poggioli T, Katsimpardi L, Buchanan SM, Oh J, Wattrus S, et al. Biochemistry and biology of GDF11 and myostatin: Similarities, differences, and questions for future investigation. Circ Res. 2016;118(7):1125–41; discussion 42. [CrossRef].
45. Shimizu K, Kikuta J, Ohta Y, Uchida Y, Miyamoto Y, Morimoto A, et al. Single-cell transcriptomics of human cholesteatoma identifies an activin A-producing osteoclastogenic fibroblast subset inducing bone destruction. Nat Commun. 2023;14(1):4417. [CrossRef].
46. Li Y, Li Y, Li L, Wang H, Wang B, Feng L, et al. The emerging translational potential of GDF11 in chronic wound healing. J Orthop Transl. 2022;34:113–20. [CrossRef].
47. Kashiwagi I, Morita R, Schichita T, Komai K, Saeki K, Matsumoto M, et al. Smad2 and Smad3 inversely regulate TGF-beta autoinduction in clostridium butyricum-activated dendritic cells. Immunity. 2015;43(1):65–79. [CrossRef].